



**HAL**  
open science

# On the Achievable Rate of Multiple-Input–Multiple-Output Underwater Acoustic Communications

Pierre-Jean Bouvet, Yves Auffret

► **To cite this version:**

Pierre-Jean Bouvet, Yves Auffret. On the Achievable Rate of Multiple-Input–Multiple-Output Underwater Acoustic Communications. *IEEE Journal of Oceanic Engineering*, 2019, 45 (3), pp.1126-1137. 10.1109/JOE.2019.2916120 . hal-02975480

**HAL Id: hal-02975480**

**<https://hal.science/hal-02975480>**

Submitted on 22 Oct 2020

**HAL** is a multi-disciplinary open access archive for the deposit and dissemination of scientific research documents, whether they are published or not. The documents may come from teaching and research institutions in France or abroad, or from public or private research centers.

L'archive ouverte pluridisciplinaire **HAL**, est destinée au dépôt et à la diffusion de documents scientifiques de niveau recherche, publiés ou non, émanant des établissements d'enseignement et de recherche français ou étrangers, des laboratoires publics ou privés.

# On the achievable rate of multiple-input multiple-output underwater acoustic communications

Pierre-Jean Bouvet\* and Yves Auffret\*

\*L@bisen, SEANERGY lab

ISEN Brest - Yncréa Ouest

Brest, France

## Abstract

This paper investigates the data gain brought by Multiple Input Multiple Output (MIMO) principle for Underwater Acoustic (UWA) communication. By considering a class of acoustic MIMO channel where each fading coefficient is modelled by a Rice distribution law with correlation factor depending on channel Doppler spread, we derive the achievable rate of such system that takes into account both channel estimation error and training sequence overhead. Model parameters are then estimated from an experiment campaign in MIMO shallow water channel conducted in the roadstead of Brest, France. The system achievable rate is evaluated for several MIMO architectures and channel configurations and then compared against conventional Single Input Multiple Output (SIMO) transmission. The achievable rate gain is finally put in perspective with end-to-end data rate performance of a single carrier MIMO transmission system experimented at sea.

## Index Terms

Underwater acoustic communications, channel capacity, information rate, MIMO.

## I. INTRODUCTION AND MOTIVATIONS

Achieving reliable UWA communications exhibits significant technical challenges due to the doubly-selective fading nature of the UWA channels that experience extremely long delay spread and fast time variation [1]–[4]. Furthermore, power consumption of UWA communication modems is clearly constrained since most of them are battery powered and it is difficult to

extend the capacity or to recharge batteries. On the other side, data rates required for UWA communications applications are continuously growing with the introduction of high-quality images, real-time video as well as the deployment of sensor networks, seafloor observatories or autonomous fleets of cooperating Autonomous Underwater Vehicle (AUV) [5], [6].

First introduced in the field of radio communications, the use of multiple transmitters and multiple receivers sharing the same frequency band, referred as MIMO, is often viewed as an efficient mean to increase spectral efficiency at same transmission power [7]–[10]. On the one hand, by transmitting multiple copies of the same information through different independently fading channels and by exploiting the different independent replica of the received signal, a spatial diversity gain is obtained that increases the reliability of the transmission. On the other hand, by transmitting multiple independent streams of information from multiple transmitters, so-called multiplexing gain, may be achieved leading to a data rate increase. According to the Shannon's theory, it has been demonstrated that the theoretical MIMO channel capacity in a scattering-rich environment increases linearly with the minimum between the number of transmit and receive antennas but the capacity gain is also shown to be strongly linked to the spatial correlation within the transmit-receive transducer array [11].

In the past ten years, researchers have deeply explored the potential of MIMO principle to improve the data rate of UWA communications and overcome the natural limitation of UWA channel. In a pioneering work, the authors of [12] demonstrated the feasibility of spatial modulation on single carrier transmission with existing equalization techniques and reported a 100-percent capacity gain with 4 transmitted streams. Associated with channel coding, spatial multiplexing with single carrier waveform is demonstrated to achieve excellent performance on UWA channel by using on the receive side linear Minimum Mean Square Error (MMSE) based iterative decoder as shown in [13]–[19]. The combination of MIMO with multi-carrier waveforms like Orthogonal Frequency Division Multiplex (OFDM) is also another attractive scheme to increase data rates in underwater acoustic channels [20]–[23]. In [20], pilot-aided channel estimation and iterative equalization are associated with two-step Doppler compensation to remove phase rotation providing a spectral efficiency up to 3.5 bit/s/Hz. In [21] the authors suggest including in the iterative loop a channel estimation algorithm exploiting the sparse structure of the UWA channel to improve performance and reduce pilot overhead, a spectral

efficiency around 5.3 bit/s/Hz is approached with 3 transmitted stream and 64-QAM constellation. While OFDM equalization enables low-complexity implementation even over highly dispersive channel, it usually requires extra guard interval (zero-padded or cyclic prefix) among transmission blocks which reduces the spectral efficiency. Moreover, the inherent sensitivity of OFDM system to Carrier Frequency Offset (CFO) makes robust signal equalization very challenging especially in mobile scenario.

In order to analyze and predict the gain brought by MIMO approach to UWA communication, MIMO UWA channel capacity has been computed and studied in various references [24]–[27]. In [24], the authors propose a first derivation of the capacity of multiple underwater acoustic channels. In [25], Radošević *et al.* compute the capacity of a MIMO system by assuming a Rician fading model while the authors of [26] evaluate the MIMO capacity from a ray tracing channel model. The MIMO underwater acoustic channel capacity gain is estimated from real experimental data in [27]. In [28], [29] the authors investigate the impact of channel estimation errors and pilot overhead on the achievable rate of OFDM based UWA communications but their analysis is limited to SIMO architecture.

In the aforementioned references [13]–[16], [18], [20], [21], either single carrier and multi-carrier MIMO UWA systems are shown to provide improved data rate with respect to their equivalent single transmitter systems but no comparison takes into account the potential robustness loss due to spatial modulation. Capacity studies provided in the literature (as shown in [24]–[27]) allow a fair comparison between MIMO and non-MIMO systems, but to the best of our knowledge, there is no existing work focusing on MIMO UWA information rate gain that assumes not perfectly known channel at the receive side but only an estimate.

The main objective of this paper is to compute a realistic rate gain brought by MIMO technology for UWA communication by taking into account the sensitivity of the receiver to time-varying nature of UWA channel. By extending recent works on the topic [27], [28], we derive a theoretical achievable rate of MIMO transmission that includes rate loss due to channel estimation error induced by fast time-varying effect like Doppler spread. Such system achievable rate is carried out on the one hand from experimental data on shallow water (based on measured channel impulse responses and time-varying estimation error) and on the other hand from UWA

MIMO synthetic channels. In order to simulate frequency and time selectivity of MIMO UWA channel fading and to derive an estimate of the channel estimation error, we consider in the present analysis a per-path Rician model as proposed in [30]–[32]. Theoretical achievable rate gains provided by UWA MIMO system over conventional SIMO transmission are then compared against performance results obtained at sea experiments and extended to various MIMO UWA channel configurations.

The paper is organized as follows: in Section II we describe the MIMO UWA system model including the transmission structure and the considered UWA channel model. In Section III we derive the theoretical achievable rate of the considered transmission system. In Section IV, rate comparison of MIMO systems against conventional single stream transmission system over simulated and experimental channels are presented whereas Section V provides comparisons w.r.t. experimental decoding performance. Finally, conclusions are summarized in VI.

## II. SYSTEM MODEL

### A. Transmission system

We consider a burst data transmission modulated around center frequency  $f_0$ . As described in Fig. 1, the frame starts with a training sequence  $x_{p,m}[k]$  of  $N_p$  symbols belonging to binary phase shift keying (BSPK) constellation with unit variance. This training sequence is used for synchronization and channel estimation and is followed by the data sequence  $x_{d,m}[k]$  including  $N_d$  data symbols belonging to a  $M$ -state Phase-Shift Keying (PSK) constellation. In order to prevent from Inter-Bloc Interference (IBI), guard interval of size  $N_g$  symbols is inserted at the end of the frame. Let us denote by  $P$  the total power of the payload signal, the passband signal transmitted through the  $m$ -th transducer can be written as:

$$s_m(t) = \Re \left[ \sqrt{P} \left\{ \sum_{u=-\infty}^{+\infty} x_m[u] g_T(t - uT) \right\} e^{j2\pi f_0 t} \right] \quad (1)$$

where  $g_T(t)$  represents the transmit pulse shaping filter chosen as Square Root Raised Cosine (SRRC) filter [33] with a roll-off factor of  $\beta$  and a symbol bandwidth of  $B = (1 + \beta)/T$  where

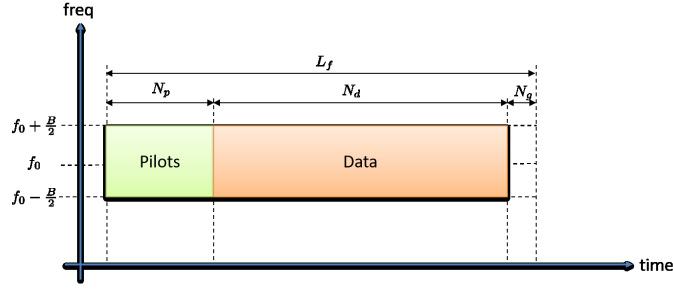


Fig. 1. Transmitted frame.

$T$  is the symbol duration. The payload frame sequence  $x_m[k]$  sent through the  $m$ -th transmitter is expressed as:

$$x_m[k] = \begin{cases} x_{p,m}[k] & k \in [1, N_p] \\ x_{d,m}[k] & k \in N_p + [1, N_d] \\ 0 & k \in N_p + N_d + [1, N_g] \end{cases} \quad (2)$$

The transmitting system considered here utilizes single carrier modulation, however we will show in Section III-A that rate analysis presented in this paper can be easily extended to multi-carrier modulations like OFDM.

### B. MIMO UWA time-varying channel

Let's assume a MIMO UWA communication channel employing  $N_t$  transmitting transducers and  $N_r$  receiving hydrophones. Due to the relative low speed of sound in water, the UWA channel is characterized by extended multipath propagation and fast time-variation brought by Doppler effect [4]. Dominant motion-induced Doppler shift is usually removed in a pre-processing stage by resampling and phase compensation [34]–[37]. At the output of such pre-processing stage, the channel frequency function linking the  $m$ -th transducer to the  $n$ -th hydrophone observed at frequency bin  $\nu$  and sampling time  $k$  can be expressed as:

$$H_{mn}[\nu, k] = \frac{1}{\sqrt{A_k}} \sum_{l=0}^{L_c-1} h_{mn}[l, k] e^{-j2\pi f_0 k T a_n[l]} e^{-j2\pi l T f_\nu} \quad (3)$$

where  $A_k$  is frequency-dependent attenuation factor (representing both absorption and spreading loss),  $h_{mn}[l, k]$  is the  $l$ -th path gain observed at sampling time  $k$  and  $a_n[l]$  is the residual motion-induced Doppler scaling factor coming from non-perfect Doppler compensation. The

frequency bins are defined as  $f_\nu = f_0 - B/2 + \nu B/N_\nu$  with  $\nu \in [0, N_\nu - 1]$ .

For the frequency bands and transmission ranges considered in the experimental results (see Section IV), the frequency dependent attenuation factor is quasi flat over the transmitted bandwidth, thus for simplicity of notation we will assume  $A_k = 1$  in the following.

As originally proposed in [32], we model each coefficient  $h_{mn}[l, k]$  as independent first order autoregressive (AR) processes obeying to following recursive equation:

$$h_{mn}[l, k] = \bar{h}_{mn}[l] + \rho_{mn}[l] \left[ h_{mn}[l, k-1] - \bar{h}_{mn}[l] \right] + \sqrt{1 - \rho_{mn}^2[l]} \sigma_{mn}[l] \chi_{mn}[l, k] \quad (4)$$

where  $\bar{h}_{mn}[l]$  is the mean value of the gain  $h_{mn}[l, k]$  whereas  $\sigma_{mn}^2[l]$  represents its variance and  $\chi_{mn}[l, k]$  is an uncorrelated noise process following a complex Normal law with zero mean and unit variance. The correlation coefficient  $\rho_{mn}[l]$  is linked to the Doppler spread  $B_{mn}^{ds}[l]$  of  $l$ -th path as [32]:

$$\rho_{mn}[l] = \exp \left( - \pi T B_{mn}^{ds}[l] \right) \quad (5)$$

With such model, for a given  $l$ , the fading coefficient gain  $|h_{mn}[l, k]|$  is demonstrated to follow a Rician distribution where the ratio  $|\bar{h}_{mn}[l]|^2 / \sigma_{mn}^2[l]$  is referred in the literature as Rician K-factor. Although no consensus exists yet on statistical UWA channel modeling (see [38], [39] and the reference herein), Rician distribution has been found to provide a good match for some UWA channel fading measurements [25], [28], [32]. We assume that channel gains are normalized such as:

$$\sum_{m=1}^{N_t} \sum_{l=0}^{L_c-1} (|\bar{h}_{mn}[l]|^2 + \sigma_{mn}^2[l]) = N_t \quad \forall n \in [1, N_r] \quad (6)$$

This power normalization is justified by the fact that transmit and receive elements are separated by 2.5 wavelengths in the experimental campaign (see Section IV-A) leading approximately to an equal average signal power for each receive streams. Finally, the residual Doppler scaling factor  $a_n[l]$  is assumed to be constant over a frame and to follow a Normal law with zero mean and variance  $\sigma_a^2$  for each path  $l$  and each receive stream  $n$  as proposed in [28].

Under these assumptions, the baseband received signal on stream  $n$  can be written as:

$$y_n[k] = \sqrt{P} \sum_{m=1}^{N_t} \sum_{l=0}^{L_c-1} h_{mn}[l, k] e^{-j2\pi f_0 k T a_n[l]} x_m[k-l] + w_n[k] \quad (7)$$

The term  $w_n[k]$  denotes the noise samples assumed to follow a complex normal law with zero mean and variance  $\sigma_w^2$ . Thus, the Signal to Noise Ratio (SNR) obtained before decoding on each receive hydrophone can be expressed in linear scale as:

$$\text{SNR} = \frac{P}{\sigma_w^2} \quad (8)$$

### III. ACHIEVABLE RATE OF MIMO UWA COMMUNICATION

#### A. Capacity and achievable rate

Let's assume that the total radiated power  $P$  is uniformly distributed across the signal bandwidth  $B$ . For simplification we will also suppose that the power spectral density (p.s.d.) of noise samples  $w_n[k]$  is flat over  $B$ . Under such assumptions, capacity of MIMO channel is given by [7], [10], [40]:

$$C = \frac{B}{N_\nu} \sum_{\nu=0}^{N_\nu-1} \log_2 \det \left[ \mathbf{I}_{N_r} + \frac{P}{N_t \sigma_w^2} \mathbf{H}[\nu, k] \mathbf{H}^H[\nu, k] \right] \quad [\text{bit/s/Hz}] \quad (9)$$

where  $\mathbf{H}[\nu, k] \in \mathbb{C}^{N_r \times N_t}$  is the MIMO channel matrix on sub-band  $\nu$  at sampling time  $k$  with entries equal to  $\{\mathbf{H}[\nu, k]\}_{n,m} = H_{mn}[\nu, k]$ . As described extensively in the literature, MIMO capacity gain is optimal if the MIMO channel matrix is sufficiently random and statistically well conditioned with the overall channel gain well distributed across the singular values [10], [26]. Eq. (9) assumes that channel state information is unknown at the transmitter. If the channel could be known at the transmit side (with for example a feedback loop), capacity could be maximized by adjusting transmit signal power as function of the frequency by using water-filling techniques [10], [28]. However, in UWA communications, the high variability and latency of the channel makes challenging any feedback from receiver to transmitter [28].

Achieving the maximum spectral efficiency stated by (9) requires at the receive side a perfect knowledge of each time-varying frequency coefficients  $\mathbf{H}[\nu, k]$  which is not realistic. In fact, in conventional MIMO UWA decoding systems, channel estimation is performed at the beginning on the transmitting frame (owing to  $N_p$  pilot symbols  $x_{p,m}[k]$  sent from  $N_t$  transmitters) and then channel coefficients are updated dynamically by using adaptive algorithms to track channel variation along the frame [15], [19], [41]. The bit rate achievable, when only the channel estimates are available, can be derived from system capacity as follows [28], [42]:

$$R = (1 - O_{vh}) \cdot \frac{B}{N_\nu} \sum_{\nu=0}^{N_\nu-1} \log_2 \det \left[ \mathbf{I}_{N_r} + \frac{P \cdot \hat{\mathbf{H}}[\nu] \cdot \hat{\mathbf{H}}^H[\nu]}{N_t(\sigma_w^2 + P\sigma_E^2)} \right] \quad (10)$$

where  $O_{vh}$  represents the overhead due to training sequence:

$$O_{vh} = \frac{N_p}{N_p + N_d} \quad (11)$$

and  $\hat{\mathbf{H}}[\nu]$  denotes the estimate of MIMO UWA channel provided by the receiver whereas parameter  $\sigma_E^2$  captures the average quality of the channel estimation along the frame that can be approximated as:

$$\sigma_E^2 = \frac{1}{N_d} \sum_{k=1}^{N_d} \sigma_E^2[k] \quad (12)$$

where  $\sigma_E^2[k]$  denotes the error variance of the channel estimation at sampling time  $k \in [1, N_d]$ . The previous parameter is linked to two factors: on the one hand the channel estimation algorithm and on the other hand the time evolution of the UWA channel. Following the notations of [28], to deal with multiple channel realizations, we denote as  $\bar{R} = \mathbb{E}\{R\}$  the average rate and  $R_{P_{out}}$  the outage rate for a given probability of outage  $P_{out} = P\{R < R_{P_{out}}\}$ .

Without loss of generality, expression (10) may be easily extended to OFDM waveform by including in  $O_{vh}$  the loss due to cyclic prefix (if any) plus pilot symbols and by particularizing parameter  $\sigma_E^2$  to OFDM channel estimation error (see [28] for more details).

### B. MIMO channel estimation

In case of Least Square (LS) estimation, the initial MIMO channel coefficients are estimated from receive pilot sequences  $\mathbf{y}_{p,n}$  as follows [43], [44]:

$$\hat{\mathbf{h}}_n = (\mathbf{X}_p^H \mathbf{X}_p)^{-1} \mathbf{X}_p^H \mathbf{y}_{p,n} \quad \forall n \in [1, N_r] \quad (13)$$

where  $\mathbf{X}_p$  is the pilot matrix of size  $(N_p - L_c + 1) \times N_t L_c$  and  $\hat{\mathbf{h}}_n$  is the channel estimates vector of size  $N_t L_c$ . In the following we will note  $\hat{h}_{mn}[l]$  the LS estimate of  $h_{mn}[l, 0]$  (and respectively  $\hat{H}_{mn}[\nu]$  in frequency domain). The Mean Square Error (MSE) provided by the LS algorithm denoted  $\sigma_{LS}^2$  is assumed equal for each sub-band  $\nu$  and is demonstrated in [10], [43] to be equal to:

$$\sigma_{LS}^2 = \frac{N_t L_c}{N_p - L_c + 1} \frac{\sigma_w^2}{P} \quad (14)$$

As expected, the channel estimation error is inversely proportional to the training sequence length  $N_p$  and the SNR. Furthermore, to achieve the same error, a MIMO system requires  $N_t$  times more training symbol than a single transmission stream system<sup>1</sup>.

### C. Time-varying channel estimation error

We define the channel estimation error variance at sampling time  $k$  as the MSE between the initial channel estimates  $\hat{H}_{mn}(\nu)$  and the real channel coefficients at sampling time  $k$ :

$$\sigma_E^2[k] = \frac{1}{N_t N_r} \sum_{m=1}^{N_t} \sum_{n=1}^{N_r} \mathbb{E} \left\{ |H_{mn}[\nu, k] - \hat{H}_{mn}[\nu]|^2 \right\} \quad (15)$$

$$= \sigma_{LS}^2 + \frac{1}{N_t N_r} \sum_{m=1}^{N_t} \sum_{n=1}^{N_r} \mathbb{E} \left\{ |H_{mn}[\nu, k] - H_{mn}[\nu, 0]|^2 \right\} \quad (16)$$

The error variance of channel estimates at sampling time  $k$  can be viewed as the sum of initial channel estimation error  $\sigma_{LS}^2$  and the average squared difference between  $H_{mn}[\nu, k]$  and  $H_{mn}[\nu, 0]$ . With the assumption of channel model described in previous section, we demonstrate in appendix A that the error evolution obeys to the following relationship:

$$\mathbb{E} \left\{ |H_{mn}[\nu, k] - H_{mn}[\nu, 0]|^2 \right\} = 2 \sum_{l=0}^{L_c-1} \left( |\bar{h}_{mn}[l]|^2 (1 - e^{-k^2 \phi^2}) + \sigma_{mn}^2[l] (1 - \rho_{mn}[l]^k) \right) \quad (17)$$

with  $\phi = \sqrt{2} \pi \sigma_a T f_0$ . As a result, the evolution of channel estimation error variance  $\sigma_E^2[k]$  is mainly influenced by resulting Doppler shift variance  $\sigma_a^2$  and channel Doppler spread  $B_{mn}^{ds}[l]$ .

### D. Upper and lower bounds

In order to study the behaviour of the achievable rate, we rewrite (10) as function of the ordered singular values  $\lambda_m[\nu]$  of  $\hat{\mathbf{H}}[\nu]$  [7]:

$$R = (1 - O_{vh}) \frac{B}{N} \sum_{\nu=0}^{N_\nu-1} \sum_{m=1}^{N_t} \log_2 \left( 1 + \frac{\text{SINR}}{N_t} \lambda_m^2[\nu] \right) \quad (18)$$

with the assumption  $N_r \geq N_t$  and  $\lambda_1[\nu] \geq \lambda_2[\nu] \geq \dots \geq \lambda_{N_t}[\nu]$ . In order to simplify the notation, we define the Signal to Interference plus Noise Ratio (SINR) as:

$$\text{SINR} = \frac{P}{\sigma_w^2 + P \sigma_E^2} \quad (19)$$

<sup>1</sup>In order to guarantee that the system equation of (13) is not under-determined, a minimum of  $N_p \geq (N_t + 1)L_c - 1$  pilot symbols are required on each transmit stream [15]

Relation (18) shows that the MIMO information rate is function of the distribution of the singular values  $\lambda_m$  that characterize the number of degrees of freedom of the channel matrix [10]. In the extreme favourable case that will constitute an upper bound on the achievable rate, all the singular values are equals, and (18) leads to a raw MIMO information rate that grows linearly with  $N_t$ . To achieve such conditions, matrix  $\hat{\mathbf{H}}$  must be sufficiently random and statistically well-conditioned which requires, in our model, the Rician  $K$  factor to tend towards 0. The MIMO channel matrix becomes Rayleigh i.i.d. meaning that each  $\hat{H}_{mn}[\nu]$  follows a Normal law with zero mean and unit variance. At moderate to high SNR, the capacity of an  $m \times m$  system is about  $m$  times the capacity of a  $1 \times 1$  system, referred as *degree of freedom* gain in the literature [10]. If such hypothesis on the channel statistics can be satisfied in radio-communications [9], we will see in the results section that this is absolutely not the case in our underwater acoustic experimentation.

In the extreme unfavourable case, all the MIMO sub-channels are correlated which require in our model the Rician  $K$  factor to tend towards  $+\infty$ . The rank of  $\hat{\mathbf{H}}$  becomes equal to 1 and the power normalization imposed in (6) leads to  $\lambda_1 = \sqrt{N_t N_r}$  and  $\lambda_m = 0$  for  $m \in [2, N_t]$ . By replacing in (18), we obtain a lower bound on the achievable rate [45]:

$$R^{LB} = (1 - O_{vh}) \frac{B}{N} \sum_{\nu=0}^{N_\nu-1} \log_2 \left( 1 + N_r \text{SINR} \right) \quad (20)$$

On the other hand, in case of SIMO transmission, the achievable rate becomes [10]:

$$R_{SIMO} = (1 - O_{vh}) \frac{B}{N} \sum_{\nu=0}^{N_\nu-1} \log_2 \left( 1 + \text{SINR} \sum_{n=1}^{N_r} |\hat{H}_{1n}[\nu]|^2 \right) \quad (21)$$

By applying again the power normalization of (6), we can easily show that if  $N_r$  is large, the average SIMO achievable rate is approximately equal to the lower bound i.e.  $\bar{R}_{SIMO} \approx R^{LB}$ . The SIMO architecture is thus demonstrated to provide a power gain w.r.t. to a single receiver system resulting in a parallel shift of the capacity versus SNR curves.

## IV. RESULTS

### A. Experimentation at Sea Test base

The experiments took place in Sea Test Base from April 27<sup>th</sup> to May 2<sup>nd</sup>, 2016. Located in the roadstead of Brest in France, the nonprofit organization Sea Test Base / Celadon [27] has deployed a coastal observatory based on an offshore experimental platform connected to the shore by a high speed WiFi link. For the project, on the one hand a 4-channel acoustic transceiver

is installed on this platform, powered by a hybrid renewable energy system, and on the other hand an 8-hydrophone acoustic receiver array is installed on a WiFi remote buoy. On each side, the transducers are equally spaced by a distance of 16.3 cm that represents 2.5 wavelengths. As depicted in Fig. 2, the projectors array is placed in vertical direction whereas the receiver array is horizontal. The embedded transmitting system is able to autonomously transmit various acoustic waveforms, the working of the system is scheduled and synchronized, and data are stored at the same time within the buoy and on a hard disk drive at the shore station. For the experiment, the transmission platform and reception buoy are separated by a range of 500 m. Depending on the tide, the water depth fluctuates between 7 m and 12 m. Fig. 3 illustrates the realized experiments.

System parameters of the experiments are summarized in Table I. We have considered two MIMO modes with 2 and 4 spatial streams respectively and a single stream conventional mode with multiple receivers denoted SIMO. The chosen center frequency  $f_0 = 23$  kHz theoretically authorizes an underwater transmission range in order of several kilometres however to guarantee high data rate for the WiFi link between the buoy and the pontoon, the transmission range is set to 500 m. For each frame, all data symbols are bit interleaved and encoded with a rate  $R_c$  Forward Error Correcting (FEC) encoder to protect information bits against channel fading and enable iterative decoding at the receive side. The FEC code considered in this paper is a 64-state convolutional code with generator polynomials of  $(133, 171)_o$ . MIMO modes employ a 4-state PSK whereas SIMO mode a 8-state PSK. The fact that a higher order constellation is used in single transmission is justified later in Section V.

For each record, 110 frames of each 3 modes are time multiplexed to ensure same channel conditions (Doppler, echoes, noise...) and perform accurate comparison between each mode. The channel delay spread is demonstrated to be in order of 5 ms, thus in the MIMO decoder we set the estimated channel length to  $L_c = 50$ . The data rate of the full system noted  $D$  is computed as follows:

$$D = \left(1 - O_{vh}\right) \frac{N_t R_c \log_2 M}{T} \quad (22)$$

As expected, by increasing  $N_t$ , the data rate  $D$  increases but so does the training sequence size  $N_p$  (since  $N_p \geq 2L_c N_t + 1$ ). Thus the increase in data rate provided by spatial multiplexing is not really linear with  $N_t$ . One can note that rate loss due to guard band is not considered here

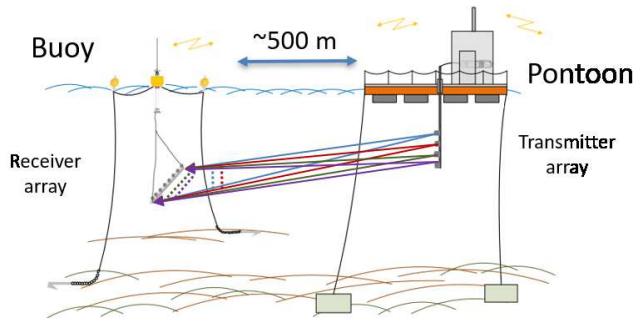


Fig. 2. Illustration of transmitter and receiver structures.

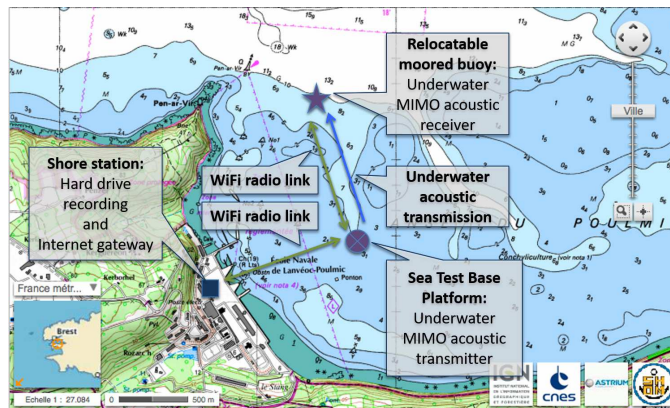


Fig. 3. Experiment scheme on Sea Test Base platform (map from Geoportail).

since it does not contribute to the signal power.

### B. Channel sounding

At the receive side, after base-band conversion, frame synchronization and Doppler compensation, MIMO LS channel estimation is performed as described in Section III-B. Fig. 4 provides the Channel Impulse Response (CIR) estimates for each sub-channel of a MIMO  $2 \times 2$  configuration during one experiment representing 110 frames with a total duration of 18 minutes, each CIR is thus separated roughly by 10 s. One can easily see on each sub-channel the large time variation that characterizes the UWA channel.

Time-evolution of the CIR coefficients within a frame, can be estimated by shifting the channel estimation window from the beginning until the end of frame as depicted in [44]. Figs 5a and 5b provide histograms of the path gain magnitude  $|h_{mn}[l, k]|$  for main path ( $l = 0$ ) and one reflected

TABLE I  
SYSTEM PARAMETERS

Notation	Parameter	Mode		
		SIMO	MIMO2	MIMO4
$N_t$	Number of transmit streams	1	2	4
$N_r$	Number of receive streams		8	
$f_0$	Center frequency [kHz]		23	
$\beta$	SRRC roll-off factor		0.4	
$B = 1/T$	Symbol bandwidth [kHz]		6.4	
$f_s$	Sampling frequency [kHz]		125	
$N_p$	Pilot symbols	150	300	600
$N_d$	Data symbols		2518	
$\mathcal{A}$	Constellation	8-PSK	QPSK	QPSK
$M$	Bits per PSK symbol	3	2	2
$R_c$	FEC rate		1/2	
$D$	Data rate [kbit/s]	8.83	11.15	20.17

path ( $l = 6$ ). For each histogram, the fitted Ricean distribution is plotted with the corresponding  $K$ -factor estimated by using the maximum likelihood method. The Ricean distribution appears to provide a good fit for all measured CIR making sense to the Rice fading assumption in the considered experiments.

Fast time variation of CIR coefficients is influenced by both small-scale fluctuations and residual motion-induced Doppler shift that are characterized in our model by Doppler spread  $B_{mn}^{ds}[l]$  and resulting Doppler shift standard deviation  $\sigma_a$ . As demonstrated in [28], the randomly varying part of the path gains,  $(h_{mn}[l, k] - \bar{h}_{mn}[l])$  is shown to fade at rate  $\rho_{mn}[l]^k \cdot e^{-k^2\phi^2}$ . It can be easily shown that for small value of time sample  $k$ , time-variation is mainly induced by  $\rho_{mn}[l]$  i.e. Doppler spread  $B_{mn}^{ds}[l]$  that can be estimated from (5) as follows:

$$B_{mn}^{ds}[l] \approx \frac{\log 2}{\pi \Delta t_{0.5}} \quad (23)$$

where  $\Delta t_{0.5}$  is the time over which the normalized correlation function of  $(h_{mn}[l, k] - \bar{h}_{mn}[l])$  drops from 1 to 0.5. For simplicity, the Doppler spread is assumed to be equal for each path of each subchannel i.e.  $B_{mn}^{ds}[l] = B^{ds}$ . In practice, parameter  $B^{ds}$  is estimated by applying (23) to the channel coherence function computed as the inverse Fourier transform of the Doppler power spectrum of  $(h_{mn}[l, k] - \bar{h}_{mn}[l])$  where  $\bar{h}_{mn}[l]$  is estimated as the slow varying mean of  $h_{mn}[l, k]$

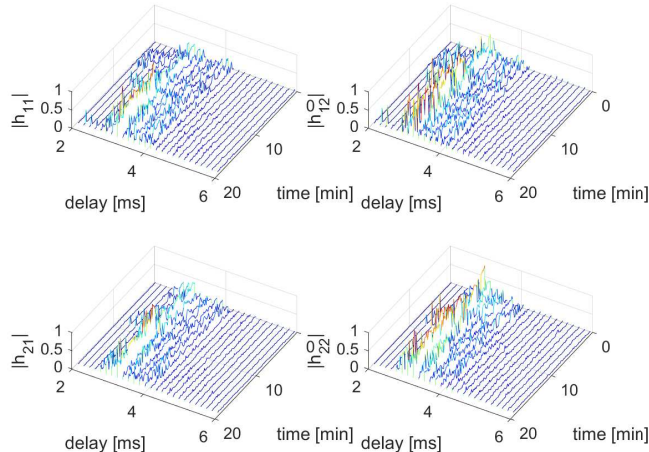


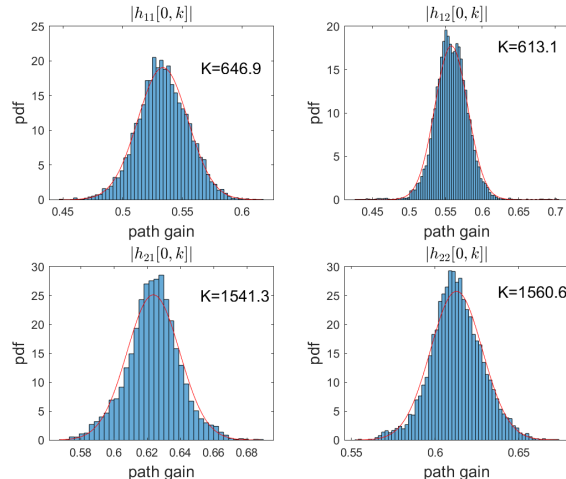
Fig. 4. Time evolution of  $|\hat{h}_{mn}[l]|$  during one experiment including 110 frames, MIMO2 mode, 500 m transmission range.

(see [46] for details). In the considered experiments, a value of  $B^{ds} = 4$  Hz is measured. On the other hand, since the average path gains  $\bar{h}_{mn}[l]$  are demonstrated to fade in our model at rate  $e^{-k^2\phi^2}$ , parameter  $\sigma_a$  can be extracted by using a similar approach but from the time coherence function of the slow varying mean  $\bar{h}_{mn}[l]$  leading to a standard deviation value in the order of  $\sigma_a f_0 = 0.1$  Hz in the considered experiments.

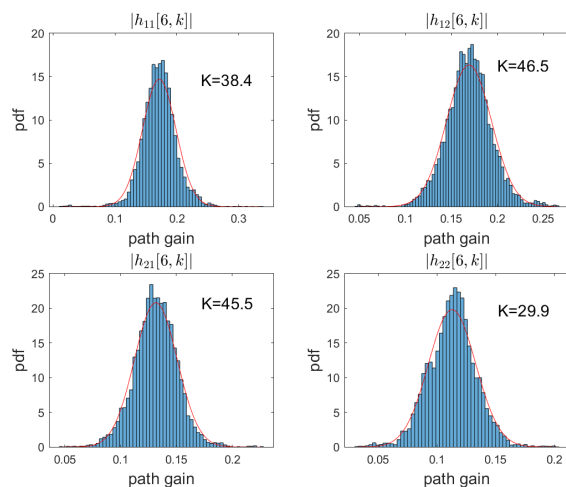
Finally, from the channel estimation process, the average noise power can be estimated frame by frame, leading for the studied experimentation to an estimated SNR oscillating between 19 and 21 dB.

### C. Achievable rate of a MIMO UWA transmission

In the following, we consider a MIMO UWA  $4 \times 8$  transmission with MIMO4 mode described in Section IV-A. In a first step, we compute the average achievable rate in case of perfect channel estimation by averaging (10) with channel frequency coefficient estimates provided by the receiver (see Fig. 4) and by fixing  $\sigma_E^2 = 0$ . The number of sub-bands is set to  $N_\nu = 640$  to obtain a frequency step of 10 Hz. The resulting average achievable rate  $\bar{R}$  relatively to the bandwidth  $B$  is plotted as function of the SNR in Fig. 6 with the solid line curve. We then replace in (10) the real channel estimates by the channel frequency coefficients obtained from the model presented in Section II where the mean gain values  $\bar{h}_{mn}[l]$  are computed according to UWA



(a) Main path



(b) Reflected path

Fig. 5. Histogram of selected path magnitude during one experiment including 110 frames, MIMO2 mode, 500 m transmission range.

channel geometry as shown in [32]. The latest channel model provides also standard deviation of each path noted as  $\tilde{\sigma}_{mn}^2[l]$ . In our model we scale these coefficients such as  $\sigma_{mn}[l] = \alpha \cdot \tilde{\sigma}_{mn}[l]$  where  $\alpha$  is determined according to the normalization constraint (6) and the average Rician factor:

$$\bar{K} = \frac{\sum_{l=0}^{L_c-1} \sigma_{mn}^2[l]}{\sum_{l=0}^{L_c-1} |h_{mn}[l]|^2} \quad (24)$$

The resulting average achievable rate is plotted in Fig. 6 as function of average Rician factor  $\bar{K}$  where a value of  $\bar{K} = 150$  is demonstrated to produce an achievable rate that matches the

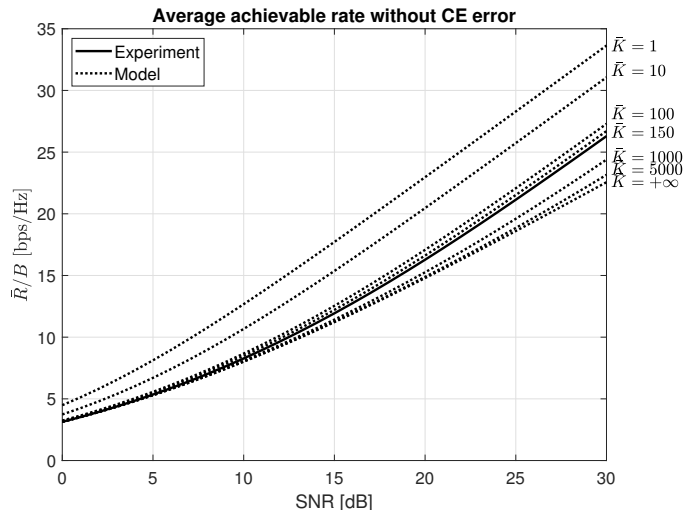


Fig. 6. Average achievable rate for UWA MIMO  $4 \times 8$  channel without channel estimation error: experiment versus model with different  $\bar{K}$  factors.

experimental one.

In a second step, we compute the channel estimation error from the experiment by rewriting (16) as function of time-varying channel frequency coefficient estimates denoted  $\hat{H}_{mn}[\nu, k]$  and  $\hat{H}_{mn}[\nu]$  yielding to the following expression:

$$\sigma_E^2[k] = \sigma_{LS}^2 + \frac{1}{N_t N_r} \sum_{m=1}^{N_t} \sum_{n=1}^{N_r} \mathbb{E} \left\{ \left| \hat{H}_{mn}[\nu, k] - \hat{H}_{mn}[\nu] \right|^2 \right\} \quad (25)$$

The resulting time-varying MSE and frame averaged error are plotted in Fig. 7 against the theoretical channel estimation error (16) obtained with model parameters estimated previously from channel soundings. We can see that theoretical curves are quite close to the experimental ones demonstrating the validity of the first order AR channel model.

In a final step, we include in equation (10) the channel estimation error on the one hand estimated from experiments and on the other hand computed from the channel model. The resulting rates are carried out in Fig. 8. For comparison purpose, we add on the same figure the achievable rates obtained without channel estimation error (see Fig. 6). Finally, as reference, we plot theoretical Rayleigh i.i.d. capacities for  $4 \times 8$  MIMO channel and  $1 \times 1$  channel respectively for which the channel coefficients  $H_{mn}[\nu, k]$  follow a complex Gaussian law with zero mean and unit variance [7]. As pinpointed in [26], the Rician characteristic of the considered UWA

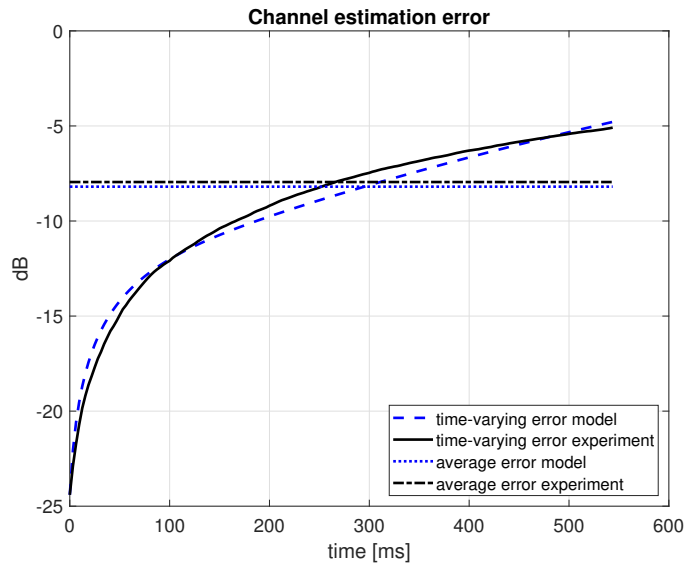


Fig. 7. Time-varying and mean errors on channel estimates over one frame, MIMO  $4 \times 8$ , 500 m range

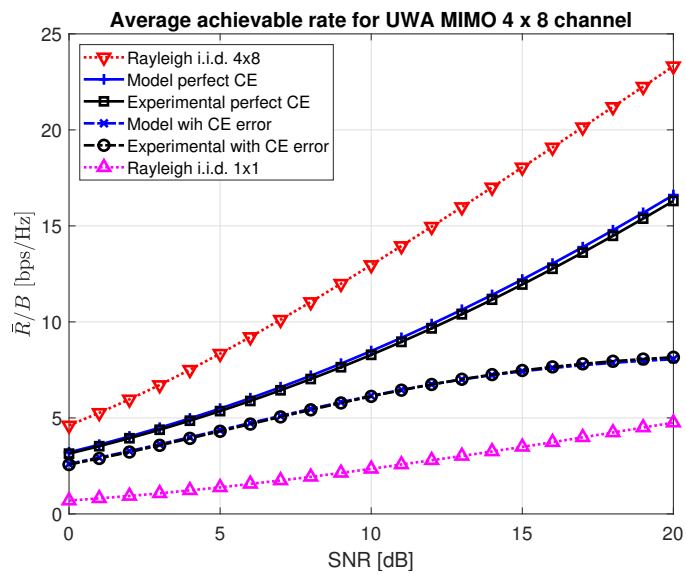


Fig. 8. Average achievable rate for UWA MIMO  $4 \times 8$  channel with and without channel estimation error: experiment versus model.

channel provides a substantial rate loss: 16.3 bps/Hz at 20 dB SNR in case of perfect channel estimation compared to 23.3 bps/Hz in case of Rayleigh i.i.d. channel. By taking into account the noise provided by the channel estimation error, the rate loss is even more significant indeed the achievable rate goes down to 8.16 bps/Hz at same SNR.

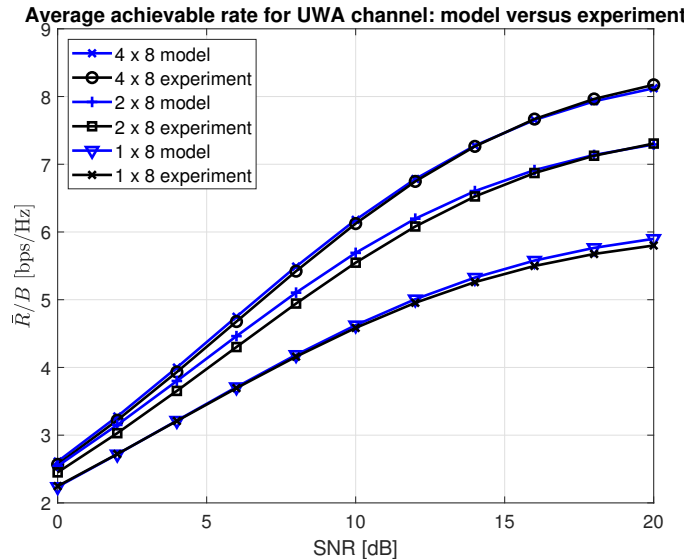


Fig. 9. Average achievable rate for UWA channel with channel estimation error for MIMO and SIMO configurations, model versus experiment.

#### D. Influence of MIMO and SIMO architectures

Fig. 10 provides respectively at SNR = 20 dB the average and 1 % outage achievable rate as function of the number of receive elements ( $N_r$ ) for different MIMO and SIMO architectures by using channel model parametrization obtained in previous section. In order to optimize the MIMO gain, we impose  $N_r \geq N_t$  for each configuration. As predicted by (20), the achievable rate of all systems grows logarithmically as function of  $N_r$  due to the so-called power gain. On the other side, one can see that the degree of freedom gain provided by spatial multiplexing increases with  $N_r$  but grows less as  $N_t$  increases.

This phenomenon is highlighted in Fig. 11 where are plotted the average and outage rate gains over SIMO defined respectively as:

$$\Delta \bar{R} = \frac{\bar{R}^{m \times n}}{\bar{R}^{1 \times n}} - 1 \quad (26)$$

and

$$\Delta R_{1\%} = \frac{R_{1\%}^{m \times n}}{R_{1\%}^{1 \times n}} - 1 \quad (27)$$

where  $\bar{R}^{m \times n}$  and  $R_{1\%}^{m \times n}$  denote the respective achievable rates for a MIMO  $m$  by  $n$  configuration. At  $N_r = 8$ , a 2-stream multiplexing scheme provides a gain about 43 %, a 3-stream scheme

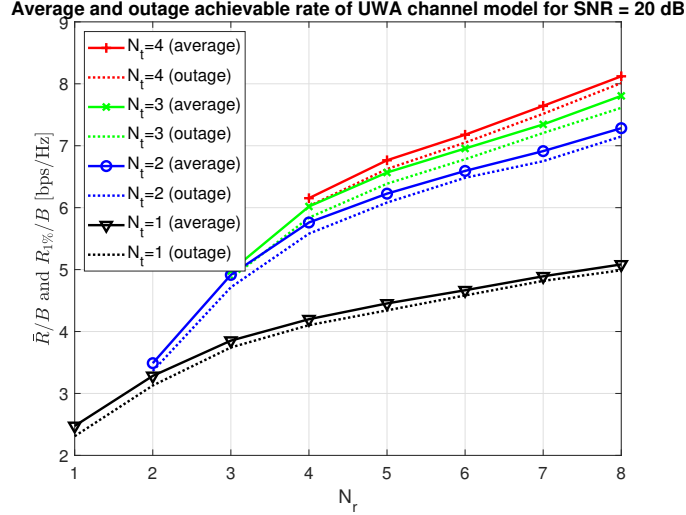


Fig. 10. Average and outage achievable rate for UWA channel model with channel estimation error as function of transmit streams and receive elements, SNR = 20 dB,  $\bar{K} = 150$ ,  $B^{ds} = 4$  Hz and  $f_d = \sigma_a f_0 = 0.1$  Hz.

about 53 % and a 4-stream scheme about 59 %. This rate gain curve is explained by two factors: first the channel estimation error that put an upper limit to the SINR and thus prevents the MIMO scheme to reach the maximum degree of freedom gain. Secondly, the overhead ratio  $O_{vh}$  that grows with  $N_t$  reduces substantially the rate gain.

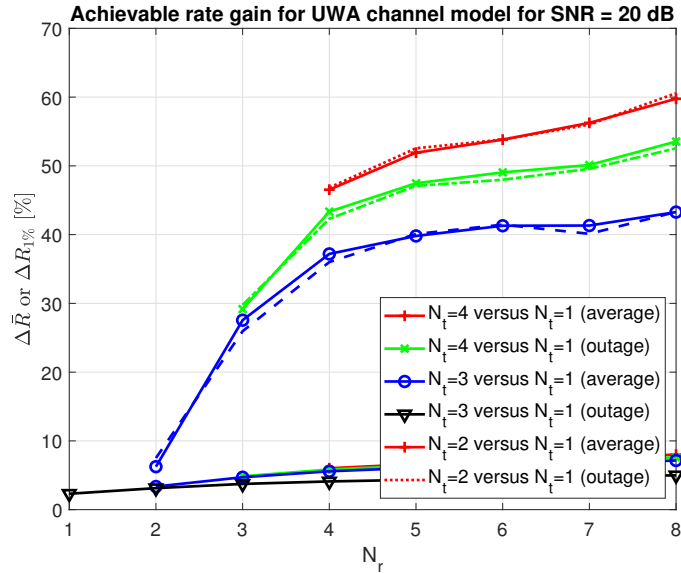


Fig. 11. Average and outage achievable rate MIMO gain over SIMO for UWA channel model with channel estimation error as function of transmit streams and receive elements, SNR = 20 dB,  $\bar{K} = 150$ ,  $B^{ds} = 4$  Hz and  $f_d = \sigma_a f_0 = 0.1$  Hz.

### E. Influence of frame length

Average and outage achievable rates of SIMO and MIMO systems against the number of data symbols per frame ( $N_d$ ) are drawn in Fig. 12 with the same channel model parameters as defined in the previous section. We can see that for small value of  $N_d$ , the overhead ratio  $O_{vh}$  becomes close to 1 and dramatically limits the achievable rate. On the opposite, by increasing  $N_d$ , relation (17) demonstrates that channel estimation error variance  $\sigma_E^2$  increases and thus limits the achievable rate. These results suggest the existence of an optimal value of  $N_d$  for which the rate is maximized that is clearly visible in aforementioned figures. By examining Fig. 13 we notice that the rate gain of MIMO grows with  $N_d$  and reaches a maximum stage for  $N_d > 2000$  in 2-stream multiplexing scheme and  $N_d > 2500$  in 4-stream multiplexing scheme. This behaviour suggests that rate loss due to an increase of the channel estimation error is noticeably equivalent for both MIMO and SIMO systems. Finally, we notice that the nominal value of  $N_d = 2500$  chosen for the experiment is demonstrated to be near optimal for MIMO data rate gain optimization. However, one can note the impact of the frame length could be efficiently mitigated by using an advanced adaptive equalization strategy like the Improved Proportionate Normalized Least Mean Squares (IPNLMS) algorithm [18].

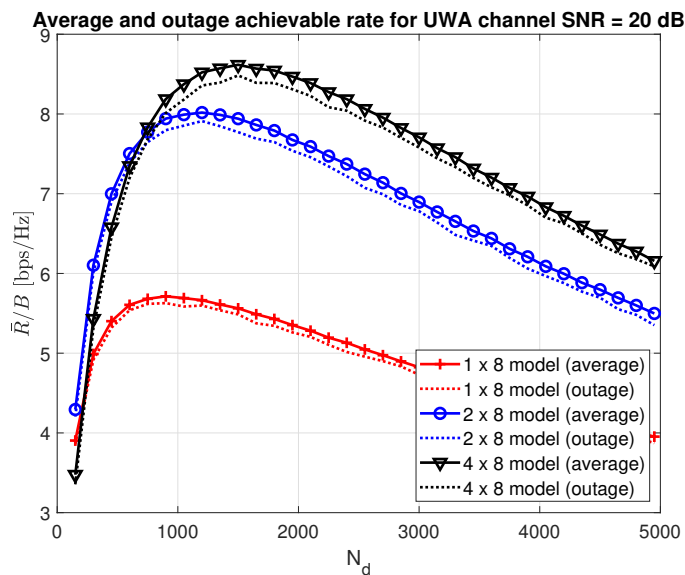


Fig. 12. Average and outage achievable rate for UWA channel model with channel estimation error as function of number of data symbols per frame ( $N_d$ ), SNR = 20 dB,  $\bar{K} = 150$ ,  $B^{ds} = 4$  Hz and  $f_d = \sigma_a f_0 = 0.1$  Hz.

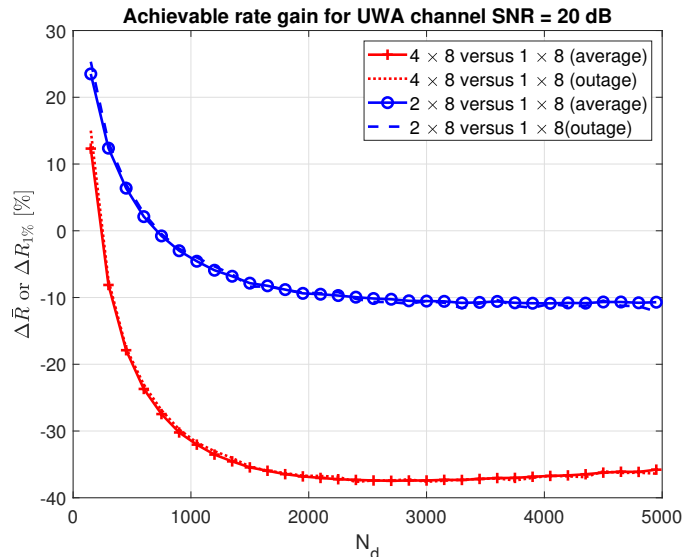


Fig. 13. Average and outage achievable rate gain of UWA MIMO channel model versus SIMO as function of number of data symbols per frame ( $N_d$ ), SNR = 20 dB,  $\bar{K} = 150$ ,  $B^{ds} = 4$  Hz and  $f_d = \sigma_a f_0 = 0.1$  Hz.

#### F. Influence of Doppler spread

In Fig. 14, we investigate the influence of Doppler spread  $B^{ds}$  to the achievable rates. In the case of the Doppler spread tends towards 0, the time coherence of the channel increases to the infinity, this leads relation (17) to converge to 0 and the channel estimation error variance to be equal to  $\sigma_{LS}^2$ . As a result achievable rates are maximized for all studied systems as we can see in the aforementioned figure. Inversely, by increasing  $B^{ds}$ , the time coherence of the channel is reduced, and the channel estimation error variance increases that leads to a rate reduction. However, the gradient of the curve is clearly lower at high Doppler spread which is explained by factor  $(1 - \rho_{mn}[l]^k)$  included in (17). A similar behaviour can be found in Fig. 15 where the average and outage achievable rate gains are plotted.

#### G. Influence of transmission range and water depth

Figs 16 and 17 provide the average achievable rate gain of MIMO  $4 \times 8$  and respectively MIMO  $2 \times 8$  over SIMO architecture as function of transmission range and water depth by using UWA channel model. For each range and water depths channel gains and delays are computed by using a geometrical approach as shown in [26] [32]. Rician and Doppler factors used for channel time variation are set identical to those measured in Section IV-B. In both cases, for a given range, we can notice that there exists a water depth for which the rate gain

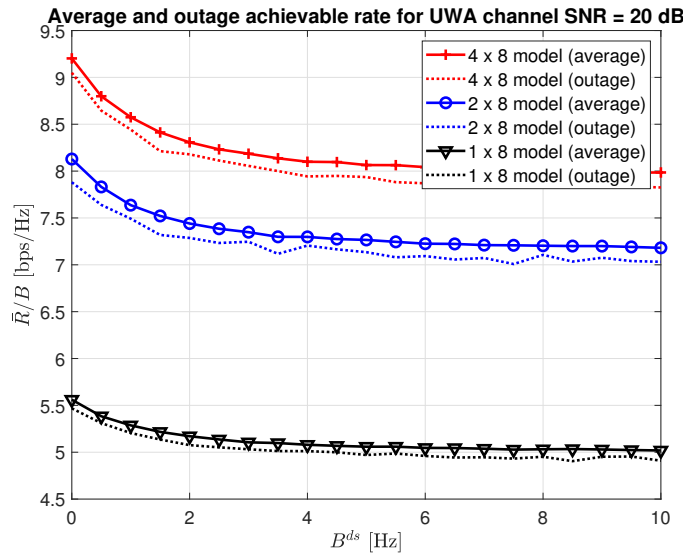


Fig. 14. Average and outage achievable rate for UWA channel model with channel estimation error as function of Doppler spread ( $B^{ds}$ ), SNR = 20 dB,  $\bar{K} = 150$ ,  $N_d = 1500$  and  $f_d = \sigma_a f_0 = 0.1$  Hz.

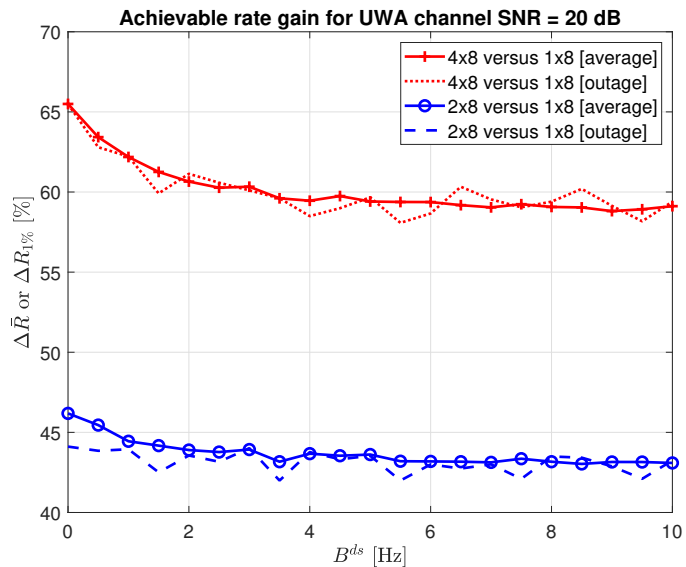


Fig. 15. Average and outage achievable rate gain of UWA MIMO channel model versus SIMO as function of Doppler spread ( $B^{ds}$ ), SNR = 20 dB,  $\bar{K} = 150$ ,  $N_d = 1500$  and  $f_d = \sigma_a f_0 = 0.1$  Hz.

is maximized. As the transmission range increases, the maximum rate gain increases too for a growing water depth: at 500 m range, the rate gain of  $4 \times 8$  mode reaches a maximum of 70 % at 20 m water depth, whereas at 5000 m range the rate gain reaches a maximum of 89 % at 95 m water depth. These phenomena are explained by the fact that as the transmission range increases

the reflected paths that provide MIMO diversity are severely attenuated leading to a near zero capacity gain in case of very shallow water channel. As both transmission range and water depth increase, the propagation time of reflected waves increases leading to higher delay spread and as a result higher MIMO capacity gain. However, at low transmission range ( $< 1000$  m), the rate gain appears in average more stable as function of water depth than at higher transmission range. As a result, MIMO transmission over very shallow water should be restricted to relative low range to maximize the rate gain over SIMO transmission.

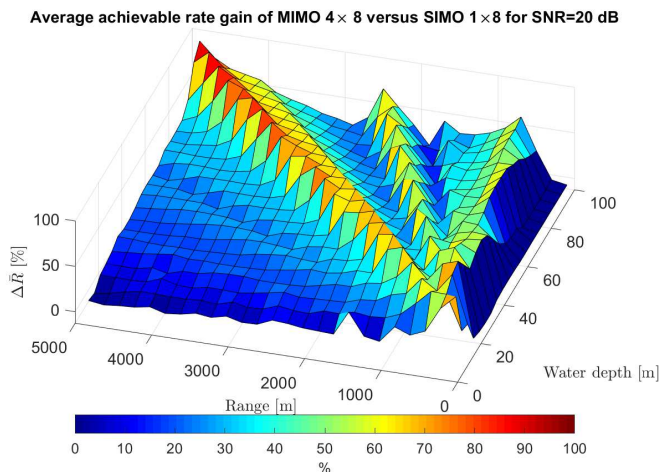


Fig. 16. Average achievable rate gain of UWA MIMO  $4 \times 8$  channel model versus SIMO  $1 \times 8$  as function of transmission range and water depth,  $B^{ds} = 4$  Hz, SNR = 20 dB,  $\bar{K} = 150$ ,  $N_d = 1500$  and  $f_d = \sigma_a f_0 = 0.1$  Hz.

## V. EXPERIMENTAL DECODING PERFORMANCE

In this section, experimental decoding performance of the SIMO and MIMO modes described in Table I are analysed and compared against the previous computed achievable rates. In the following, we consider the iterative equalizer described in a previous paper [41] that takes as inputs on the one-hand the pre-processed symbols  $y_n[k]$  with  $n \in [1, N_r]$  and  $k \in [1, N_d]$  and on the other side the MIMO channel estimates  $\hat{h}_{mn}[l]$  with  $m \in [1, N_t]$  and  $l \in [0, L_c - 1]$ . The iterative equalizer is based on the turbo-equalization principle and optimized under MMSE criterion [47]. A residual Doppler phase correction algorithm [17] is also performed at each iteration by estimating and averaging the symbol phase rotation along a block of symbols to track residual phase shift along the frame.

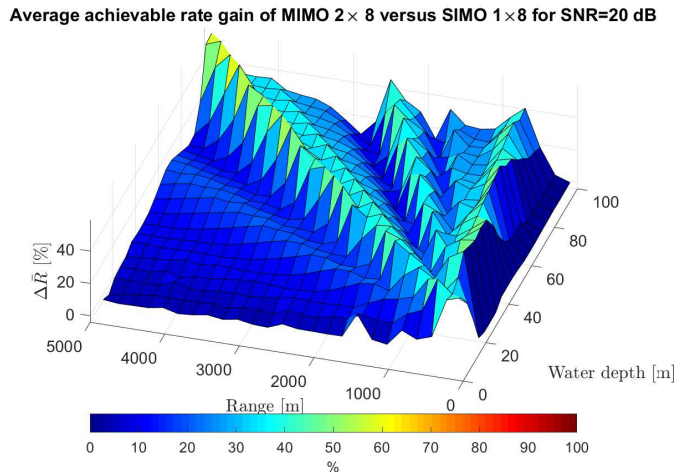


Fig. 17. Average achievable rate gain of UWA MIMO 2 × 8 channel model versus SIMO 1 × 8 as function of transmission range and water depth,  $B^{ds} = 4$  Hz, SNR = 20 dB,  $\bar{K} = 150$ ,  $N_d = 1500$  and  $f_d = \sigma_a f_0 = 0.1$  Hz.

In order to measure the performance of equalization scheme we compute the MSE between the equalized symbols  $\hat{x}_m[k]$  and the transmitted ones  $x_m[k]$  as follows:

$$\epsilon^2[k] = \frac{1}{N_t} \sum_{m=1}^{N_t} \mathbb{E}\{|\hat{x}_m[k] - x_m[k]|^2\} \quad (28)$$

In [41] [48], it was demonstrated that the MSE of a turbo-equalizer tends towards the following optimum bound:

$$\epsilon_{opt}^2[k] = \text{SINR} \cdot \frac{N_r}{N_t} \quad (29)$$

$$= \frac{P}{\sigma_w^2 + P\sigma_E^2[k]} \cdot \frac{N_r}{N_t} \quad (30)$$

where factor  $N_r/N_t$  represents the so-called array power gain. From (30), we can easily demonstrate that at same number of receivers, a 2-transmitter MIMO mode exhibits a 3 dB SNR penalty w.r.t. SIMO mode. This fact justifies the use of 8-state PSK in case of SIMO to achieve roughly the same robustness as 4-state PSK signalling in 2 spatial streams MIMO mode, and thus to make as honest as possible the rate comparison between SIMO and MIMO2 modes.

In Fig. 18, the experimental values of  $\epsilon^2[k]$  are carried out as function of symbol index for the SIMO, MIMO2 and MIMO4 modes. The MSE metrics are obtained by averaging on 110 successive frames the squared estimation error for each symbol index  $k$ . On the same figure,

the optimal MSE computed from (30) is plotted for the three transmission architectures. The experimental MSE follows the same slope as the optimal ones and especially for the MIMO2 and SIMO modes, the equalization MSEs are really closed to the optimal bounds. These facts demonstrate the validity of  $\sigma_E[k]^2$  definition in (16) to model the channel estimation error. For the  $4 \times 8$  architecture, we notice that the equalizer performance remains far away from the optimal bound showing that the iterative process is not able to remove the whole spatial interferences. Moreover, the equalization performances allow to verify the power gain stated in (30) i.e.  $1 \times 8$  scheme is 3 dB better in MSE than the  $2 \times 8$  scheme that is itself 3 dB better in MSE than the  $4 \times 8$  scheme [10] [41].

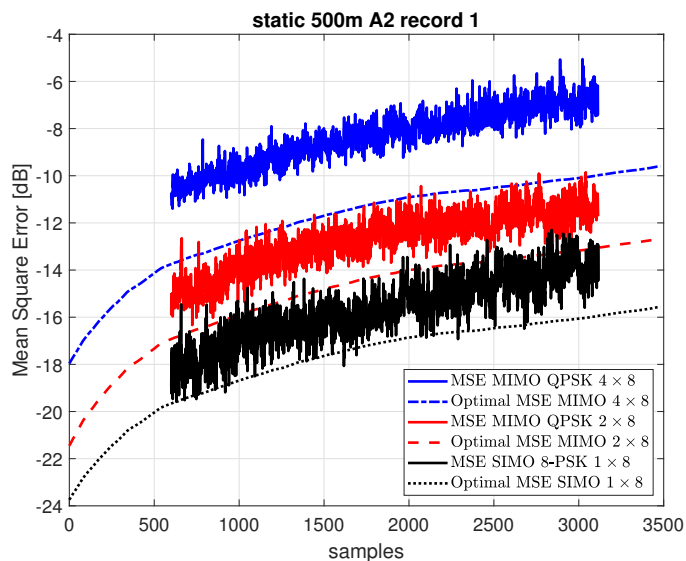


Fig. 18. Experimental MSE at the equalizer output averaged on 110 frames versus optimal MSE computed from  $\sigma_E^2[k]$  based on channel model with  $B^{ds} = 4$  Hz, SNR = 20 dB,  $\bar{K} = 150$  and  $f_d = \sigma_a f_0 = 0.1$  Hz.

Fig. 19 provides Bit Error Rate (BER) decoding results of the 3 modes by using the experimental records described in Section IV-A that represents roughly 18 minutes of experiment for which the time-varying CIR is plotted in Fig. 4. For each mode, we compute the effective data rate  $D_e$  as:

$$D_e = (1 - \text{PER})D \quad (31)$$

where PER denotes the packet error ratio. A packet is said erroneous if at least one erroneous bit per frame is detected at the output the decoder. The achieved PER is 2.7 %, 0 % and 1.8 % for MIMO4, MIMO2 and SIMO modes respectively. By comparing decoding performance

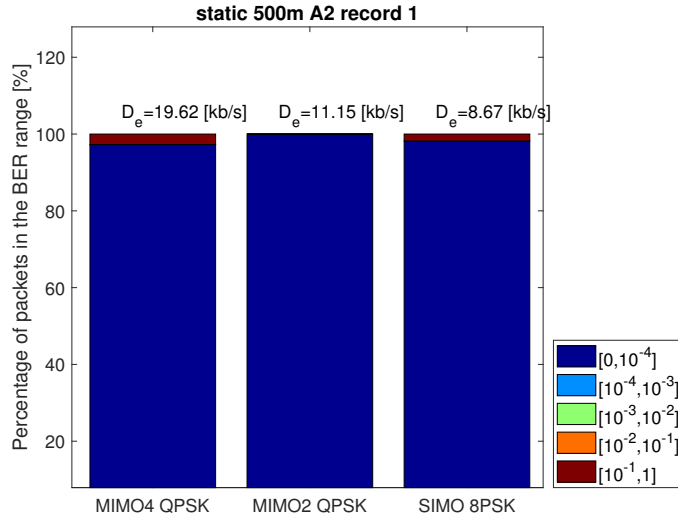


Fig. 19. BER decoding performance comparison on static experimentation.

of MIMO2 and SIMO modes, we notice a net data rate gain for MIMO of 29 %. Since the robustness of the SIMO transmission with 8-PSK constellation is lower than the MIMO2 one with QPSK constellation, the practical rate gain at quasi-error free decoding is expected to be greater than 29 % which is coherent with 43 % gain in achievable rate computed in Fig. 11.

Fig. 20 provides performance results of the same modes but in a dynamic scenario. In this experiment, the receive buoy is not anchored and is drifting away from the pontoon due to sea currents. Moreover, since the buoy was moving quite fast out of the range of the WiFi link, the experiment was stopped after 6 minutes of recording. The achieved PER is 8.3 %, 0 % and 8.3 % for respectively MIMO4, MIMO2 and SIMO modes. As expected, the motion-induced Doppler effect provides performance degradation especially for MIMO4 and SIMO modes but the number of correct decoded frames still remains in a majority proportion demonstrating the ability of the considered MIMO receiver to deal with Doppler effect. By comparing again decoding performance of MIMO2 and SIMO modes, we notice a net data rate gain for MIMO of 34 % that is quite closed to the gain obtained in the static scenario and again coherent with achievable rate gain in Fig. 11. However, the practical spectral efficiencies are 3.15, 1.74 and 1.37 bps/Hz for MIMO4, MIMO2 and SIMO modes respectively which are far away from the theoretical achievable rates  $\bar{R}/B$  and  $R_{1\%}/B$ . This gap could be explained by the fact that the achievable rate computed in this paper still remains a theoretical asymptomatic bound that does

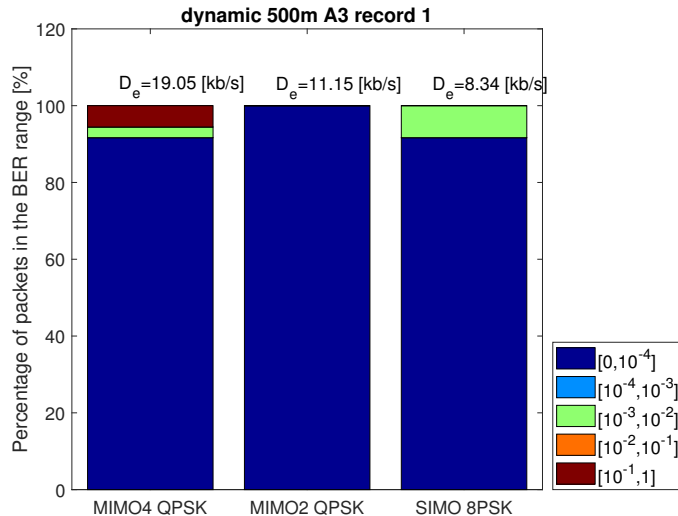


Fig. 20. BER decoding performance comparison on dynamic experimentation.

not take into account for example limitation due to FEC coding (finite blocklength codeword will substantially impact the achievable rate, see [49] for details). Moreover the convolutional coding scheme adopted for this study is much less powerful than near-capacity FEC coding scheme like turbo-codes or Low Density Parity Check (LDPC) code [16].

## VI. CONCLUSION AND DISCUSSIONS

The primary aim of this study was to quantify the data rate gain brought by MIMO technology for UWA communication. By deriving the MIMO Shannon's capacity, we compute a theoretical achievable rate of MIMO UWA single-carrier transmission system that takes into account rate loss due to time-varying channel estimation error. By assuming that each equivalent channel coefficient follows a Rice law and obeys to a first order AR model as suggested in [32], we derive the channel estimation error variance for the MIMO case. From experimental records performed in very shallow water in the roadstead of Brest (France), MIMO channel coefficients are estimated as well as Rician factor and Doppler spread leading to theoretical achievable rate as function of number of transmitters and receivers. Although our study focuses on single-carrier UWA transmission, the analysis can be easily extended without any loss of generality to other waveforms like OFDM for example. In contrary to radio communication on earth, the MIMO achievable rate for the UWA channel is demonstrated to grow logarithmically with the number of transmit streams to achieve 43 % and 59 % gain in  $2 \times 8$  and  $4 \times 8$  configurations respectively

for the studied experiment that is mostly explained by the Rician nature and the time-varying properties of the UWA channel. We show also that the MIMO rate gain is very sensitive to channel geometry and even the MIMO rate gain is maximized by increasing both range and water depth, relative low transmission range over shallow water ensures substantial capacity gain whatever the water depth. Decoding performance of the experimental records confirm the feasibility of underwater acoustic MIMO transmission as already depicted in the literature but spectral efficiencies reached in practice are still far below the absolute values of theoretical achievable rates demonstrating that there is room for transmission performance enhancement. However decoding performance comparison between MIMO and SIMO modes suggests that effective data rate gain brought by MIMO in UWA transmission lies in the same range as theoretical achievable rate gain computed in this paper that confirms MIMO technique as a key technology to improve spectral efficiency of UWA communications.

## APPENDIX A

### TIME-VARYING ERROR ON CHANNEL ESTIMATION

The following demonstration is a generalization of [28] to the MIMO case. In fact, for a given  $m \in [1, N_t]$  and  $n \in [1, N_r]$ , we can write:

$$\begin{aligned} \mathbb{E}\left\{|H_{mn}[\nu, k] - H_{mn}[\nu, 0]|^2\right\} &= \mathbb{E}\left\{|H_{mn}[\nu, k]|^2\right\} + \mathbb{E}\left\{|H_{mn}[\nu, 0]|^2\right\} \\ &\quad - 2\mathbb{E}\left\{H_{mn}[\nu, k]H_{mn}^*[\nu, 0]\right\} \end{aligned} \quad (32)$$

With the power normalization stated in (6), the application of Paserval's theorem leads to:

$$\mathbb{E}\left\{|H_{mn}[\nu, k]|^2\right\} = \mathbb{E}\left\{|H_{mn}[\nu, 0]|^2\right\} = \sum_{l=0}^{L_c-1} \left(|\bar{h}_{mn}[l]|^2 + \sigma_{mn}^2[l]\right) \quad (33)$$

On the otherside, the correlation factor may be expanded as:

$$\begin{aligned} \mathbb{E}\left\{H_{mn}[\nu, k]H_{mn}^*[\nu, 0]\right\} &= \mathbb{E}\left\{\sum_l h_{mn}[l, k]e^{-j2\pi f_0 k T a_n[l]}e^{-j2\pi l T f_\nu} \cdot \sum_{l'} h_{mn}^*[l', 0]e^{j2\pi l' T f_\nu}\right\} \\ &= \sum_l \sum_{l'} \mathbb{E}_H\{h_{mn}[l, k]h_{mn}^*[l', 0]\} \cdot \mathbb{E}_H\{e^{-j2\pi f_0 k T a_n[l]}\} \end{aligned} \quad (34)$$

By assuming that channel paths are uncorrelated, we can write

$$\mathbb{E}_H\{h_{mn}[l, k]h_{mn}^*[l', 0]\} = \begin{cases} |\bar{h}_{mn}[l]|^2 + \rho_{mn}[l]^k \sigma_{mn}^2[l] & \text{if } l = l' \\ 0 & \text{if } l \neq l' \end{cases} \quad (35)$$

On the other hand, with the assumption that  $a_n[l]$  follows a zero mean normal law with variance  $\sigma_a^2$ , it yields:

$$\begin{aligned}\mathbb{E}\left\{e^{-j2\pi f_0 k T a_n[l]}\right\} &= \int_{-\infty}^{+\infty} e^{-j2\pi f_0 k T a_n[l]} \frac{e^{-(a_n[l])^2/2\sigma_a^2}}{\sigma_a\sqrt{2\pi}} da_n[l] \\ &= e^{-k^2\phi^2}\end{aligned}$$

with  $\phi = \sqrt{2\pi}\sigma_a T f_0$ . By combining previous expressions, we finally obtain:

$$\begin{aligned}\mathbb{E}_H\left\{\left|H_{mn}[\nu, k] - H_{mn}[\nu]\right|^2\right\} &= 2 \sum_{l=0}^{L_c-1} \left(\left|\bar{h}_{mn}[l]\right|^2 + \sigma_{mn}^2[l]\right) - 2e^{-k^2\phi^2} \sum_{l=0}^{L_c-1} \left(\left|\bar{h}_{mn}[l]\right|^2 + \rho_{mn}[l]^k \sigma_{mn}^2[l]\right) \\ &= 2 \sum_{l=0}^{L_c-1} \left(\left|\bar{h}_{mn}[l]\right|^2 (1 - e^{-k^2\phi^2}) + \sigma_{mn}^2[l] (1 - \rho_{mn}[l]^k)\right)\end{aligned}\quad (36)$$

#### ACKNOWLEDGMENT

The authors would like to thank R. Bourdon, J. Janvresse, P. Tessot and Y. Eustache from NEOTEK RTSYS and A. Pottier and D. Munck from Sea Test Base who conducted together the experiment campaign described in this paper in the framework of the project RAPID MA-MIMO supported by the french General Directorate for Armament for Naval Techniques (DGA / TN).

#### REFERENCES

- [1] M. Stojanovic, "Acoustic (Underwater) Communications," in *Wiley Encyclopedia of Telecommunications*. John Wiley & Sons, Inc., 2003. [Online]. Available: <http://onlinelibrary.wiley.com/doi/10.1002/0471219282.eot110/abstract>
- [2] M. Stojanovic and J. Preisig, "Underwater acoustic communication channels: Propagation models and statistical characterization," *IEEE Communications Magazine*, vol. 47, no. 1, pp. 84–89, Jan. 2009.
- [3] T. C. Yang, "Properties of underwater acoustic communication channels in shallow water," *The Journal of the Acoustical Society of America*, vol. 131, no. 1, pp. 129–145, Jan. 2012.
- [4] M. Stojanovic and P.-P. J. Beaujean, "Acoustic Communication," in *Springer Handbook of Ocean Engineering*, M. R. Dhanak and N. I. Xiros, Eds. Springer International Publishing, 2016, pp. 359–386.
- [5] M. Chitre, S. Shahabudeen, and M. Stojanovic, "Underwater Acoustic Communications and Networking: Recent Advances and Future Challenges," *Marine Technology Society Journal*, vol. 42, no. 1, pp. 103–116, Mar. 2008.
- [6] T. Melodia, H. Kulhandjian, L.-C. Kuo, and E. Demirors, "Advances in Underwater Acoustic Networking," in *Mobile Ad Hoc Networking*, S. Basagni, r. Conti, S. Giordano, and I. Stojmenovic, Eds. John Wiley & Sons, Inc., 2013, pp. 804–852. [Online]. Available: <http://onlinelibrary.wiley.com/doi/10.1002/9781118511305.ch23/summary>
- [7] E. Telatar, "Capacity of Multi-antenna Gaussian Channels," *European transactions on telecommunications*, vol. 10, no. 6, pp. 585–595, 1999. [Online]. Available: <http://onlinelibrary.wiley.com/doi/10.1002/ett.4460100604/full>
- [8] D. Gesbert, M. Shafi, D.-s. Shiu, P. J. Smith, and A. Naguib, "From theory to practice: an overview of MIMO space-time coded wireless systems," *IEEE Journal on Selected Areas in Communications*, vol. 21, no. 3, pp. 281–302, Apr. 2003.

- [9] A. J. Paulraj, D. A. Gore, R. U. Nabar, and H. Bolcskei, "An overview of MIMO communications - a key to gigabit wireless," *Proceedings of the IEEE*, vol. 92, no. 2, pp. 198–218, Feb. 2004.
- [10] D. Tse and P. Viswanath, *Fundamentals of Wireless Communication*. Cambridge University Press, 2005.
- [11] C.-N. Chuah, D. N. C. Tse, J. M. Kahn, and R. A. Valenzuela, "Capacity scaling in MIMO wireless systems under correlated fading," *IEEE Transactions on Information Theory*, vol. 48, no. 3, pp. 637–650, Mar. 2002.
- [12] D. B. Kilfoyle, J. C. Preisig, and A. B. Baggeroer, "Spatial modulation experiments in the underwater acoustic channel," *IEEE Journal of Oceanic Engineering*, vol. 30, no. 2, pp. 406–415, Apr. 2005.
- [13] S. Roy, T. M. Duman, V. McDonald, and J. G. Proakis, "High-Rate Communication for Underwater Acoustic Channels Using Multiple Transmitters and Space-Time Coding: Receiver Structures and Experimental Results," *IEEE Journal of Oceanic Engineering*, vol. 32, no. 3, pp. 663–688, Jul. 2007.
- [14] J. W. Choi, T. J. Riedl, K. Kim, A. C. Singer, and J. C. Preisig, "Adaptive Linear Turbo Equalization Over Doubly Selective Channels," *IEEE Journal of Oceanic Engineering*, vol. 36, no. 4, pp. 473–489, Oct. 2011.
- [15] J. Tao, J. Wu, Y. R. Zheng, and C. Xiao, "Enhanced MIMO LMMSE Turbo Equalization: Algorithm, Simulations, and Undersea Experimental Results," *IEEE Transactions on Signal Processing*, vol. 59, no. 8, pp. 3813–3823, Aug. 2011.
- [16] A. Rafati, H. Lou, and C. Xiao, "Soft-Decision Feedback Turbo Equalization for LDPC-Coded MIMO Underwater Acoustic Communications," *IEEE*, vol. 39, no. 1, pp. 90–99, Jan. 2014.
- [17] Y. R. Zheng, J. Wu, and C. Xiao, "Turbo equalization for single-carrier underwater acoustic communications," *IEEE Communications Magazine*, vol. 53, no. 11, pp. 79–87, Nov. 2015.
- [18] Z. Yang and Y. R. Zheng, "Iterative Channel Estimation and Turbo Equalization for Multiple-Input Multiple-Output Underwater Acoustic Communications," *IEEE Journal of Oceanic Engineering*, vol. 41, no. 1, pp. 232–242, Jan. 2016.
- [19] Z. Chen, J. Wang, and Y. R. Zheng, "Frequency-Domain Turbo Equalization With Iterative Channel Estimation for MIMO Underwater Acoustic Communications," *IEEE Journal of Oceanic Engineering*, vol. PP, no. 99, pp. 1–11, 2016.
- [20] B. Li, S. Zhou, M. Stojanovic, L. Freitag, and P. Willett, "Multicarrier Communication Over Underwater Acoustic Channels With Nonuniform Doppler Shifts," *IEEE Journal of Oceanic Engineering*, vol. 33, no. 2, pp. 198–209, Apr. 2008.
- [21] J. Huang, J. Huang, C. Berger, S. Zhou, and P. Willett, "Iterative Sparse Channel Estimation and Decoding for Underwater MIMO-OFDM," *EURASIP Journal on Advances in Signal Processing*, vol. 2010, no. 1, p. 460379, 2010. [Online]. Available: <http://asp.eurasipjournals.com/content/2010/1/460379>
- [22] C.-F. Lin, S.-H. Chang, C.-C. Lee, W.-C. Wu, W.-H. Chen, K.-H. Chang, J.-Y. Lee, and I. A. Parinov, "Underwater Acoustic Multimedia Communication Based on MIMO-OFDM," *Wireless Personal Communications*, vol. 71, no. 2, pp. 1231–1245, 2013. [Online]. Available: <http://dx.doi.org/10.1007/s11277-012-0871-4>
- [23] G. Qiao, Z. Babar, L. Ma, S. Liu, and J. Wu, "MIMO-OFDM underwater acoustic communication systems : a review," *Physical Communication*, vol. 23, pp. 56–64, Jun. 2017. [Online]. Available: <http://www.sciencedirect.com/science/article/pii/S1874490716301550>
- [24] T. J. Hayward and T. C. Yang, "Single- and multi-channel underwater acoustic communication channel capacity: A computational study," *J Acoust Soc Am*, vol. 122, no. 3, pp. 1652–1661, 2007. [Online]. Available: <http://scitation.aip.org/content/asa/journal/jasa/122/3/10.1121/1.2749709>
- [25] A. Radošević, D. Fertoni, T. Duman, J. Proakis, and M. Stojanovic, "Capacity of MIMO Systems in Shallow Water Acoustic Channels," in *Proc. 43rd Asilomar Conference on Signals, Systems and Computers*, Nov. 2009.
- [26] P. J. Bouvet and A. Loussert, "Capacity analysis of underwater acoustic MIMO communications," in *OCEANS 2010 IEEE - Sydney*, May 2010, pp. 1–8.

- [27] P. J. Bouvet, Y. Auffret, A. Loussert, P. Tessot, G. Janvresse, and R. Bourdon, "MIMO underwater acoustic channel characterization based on a remotely operated experimental platform," in *OCEANS 2014 - TAIPEI*, Apr. 2014, pp. 1–6.
- [28] Y. M. Aval, S. K. Wilson, and M. Stojanovic, "On the Achievable Rate of a Class of Acoustic Channels and Practical Power Allocation Strategies for OFDM Systems," *IEEE Journal of Oceanic Engineering*, vol. 40, no. 4, pp. 785–795, Oct. 2015.
- [29] —, "On the Average Achievable Rate of QPSK and DQPSK OFDM Over Rapidly Fading Channels," *IEEE Access*, vol. 6, pp. 23 659–23 667, 2018.
- [30] A. Radosevic, J. G. Proakis, and M. Stojanovic, "Statistical characterization and capacity of shallow water acoustic channels," in *OCEANS 2009-EUROPE*, May 2009, pp. 1–8.
- [31] J. M. Passerieux, F. X. Socheleau, and C. Laot, "Achievable Rates over Doubly Selective Rician-Fading Channels under Peak-Power Constraint," *IEEE Transactions on Wireless Communications*, vol. 12, no. 2, pp. 586–594, Feb. 2013.
- [32] P. Qarabaqi and M. Stojanovic, "Statistical Characterization and Computationally Efficient Modeling of a Class of Underwater Acoustic Communication Channels," *IEEE Journal of Oceanic Engineering*, vol. 38, no. 4, pp. 701–717, Oct. 2013.
- [33] J. G. Proakis and M. Salehi, *Digital Communications Sed*, 5th ed. Boston, Mass.: McGraw-Hill, 2008.
- [34] B. S. Sharif, J. Neasham, O. R. Hinton, and A. E. Adams, "A computationally efficient Doppler compensation system for underwater acoustic communications," *IEEE Journal of Oceanic Engineering*, vol. 25, no. 1, pp. 52–61, Jan. 2000.
- [35] T. H. Eggen, A. B. Baggeroer, and J. C. Preisig, "Communication over Doppler spread channels. Part I: Channel and receiver presentation," *IEEE Journal of Oceanic Engineering*, vol. 25, no. 1, pp. 62–71, Jan. 2000.
- [36] G. Eynard and C. Laot, "Blind Doppler compensation scheme for single carrier digital underwater communications," in *OCEANS 2008*, Sep. 2008, pp. 1–5.
- [37] L. Wan, Z. Wang, S. Zhou, T. C. Yang, and Z. Shi, "Performance Comparison of Doppler Scale Estimation Methods for Underwater Acoustic OFDM," *Journal of Electrical and Computer Engineering*, vol. 2012, p. e703243, May 2012. [Online]. Available: <https://www.hindawi.com/journals/jece/2012/703243/abs/>
- [38] P. A. v. Walree, T. Jenserud, and M. Smedsrud, "A Discrete-Time Channel Simulator Driven by Measured Scattering Functions," *IEEE Journal on Selected Areas in Communications*, vol. 26, no. 9, pp. 1628–1637, Dec. 2008.
- [39] F. X. Socheleau, C. Laot, and J. M. Passerieux, "A maximum entropy framework for statistical modeling of underwater acoustic communication channels," in *OCEANS 2010 IEEE - Sydney*, May 2010, pp. 1–7.
- [40] A. Goldsmith, S. A. Jafar, N. Jindal, and S. Vishwanath, "Capacity limits of MIMO channels," *IEEE Journal on Selected Areas in Communications*, vol. 21, no. 5, pp. 684–702, Jun. 2003.
- [41] P. J. Bouvet, Y. Auffret, D. Munck, A. Pottier, G. Janvresse, Y. Eustache, P. Tessot, and R. Bourdon, "Experimentation of MIMO underwater acoustic communication in shallow water channel," in *OCEANS 2017 IEEE - Aberdeen*, Jun. 2017, pp. 1–8.
- [42] T. Yoo and A. Goldsmith, "Capacity and power allocation for fading MIMO channels with channel estimation error," *IEEE Transactions on Information Theory*, vol. 52, no. 5, pp. 2203–2214, May 2006.
- [43] J. A. Flynn, J. A. Ritcey, D. Rouseff, and W. L. J. Fox, "Multichannel equalization by decision-directed passive phase conjugation: experimental results," *IEEE Journal of Oceanic Engineering*, vol. 29, no. 3, pp. 824–836, Jul. 2004.
- [44] S. Kaddouri, P. P. J. Beaujean, P. J. Bouvet, and G. Real, "Least Square and Trended Doppler Estimation in Fading Channel for High-Frequency Underwater Acoustic Communications," *IEEE Journal of Oceanic Engineering*, vol. 39, no. 1, pp. 179–188, Jan. 2014.
- [45] G. Lebrun, M. Faulkner, M. Shafi, and P. J. Smith, "MIMO Ricean channel capacity: an asymptotic analysis," *IEEE Transactions on Wireless Communications*, vol. 5, no. 6, pp. 1343–1350, Jun. 2006.

- [46] P. van Walree, "Channel sounding for acoustic communications: techniques and shallow-water examples," *Norwegian Defence Research Establishment (FFI), Tech. Rep. FFI-rapport*, vol. 7, 2011.
- [47] M. Tuchler, A. C. Singer, and R. Koetter, "Minimum mean squared error equalization using a priori information," *IEEE Transactions on Signal Processing*, vol. 50, no. 3, pp. 673–683, Mar. 2002.
- [48] C. Laot, R. L. Bidan, and D. Leroux, "Low-complexity MMSE turbo equalization: a possible solution for EDGE," *IEEE Transactions on Wireless Communications*, vol. 4, no. 3, pp. 965–974, May 2005.
- [49] P. Mary, J. Gorce, A. Unsal, and H. V. Poor, "Finite Blocklength Information Theory: What Is the Practical Impact on Wireless Communications?" in *2016 IEEE Globecom Workshops (GC Wkshps)*, Dec. 2016, pp. 1–6.



**Pierre-Jean Bouvet** (M10) was born in Clermont-Ferrand, France, in 1978. He received the dipl.-ing. and Ph. D degrees in electrical engineering from the National Institute of Applied Science (INSA) Rennes, France, in 2001 and 2005, respectively.

In 2005, he joined NXP semiconductors (formerly Philips) in Caen, France, as baseband decoding architect for digital TV demodulator products (DVB-T/T2). Since 2009, he has been an associate professor in the department of embedded systems, acoustic and communications in the engineering college of ISEN, Brest, France. His current research interests include underwater acoustic communications, underwater network, MIMO transmission, iterative reception, synchronization and localization algorithms.



**Yves Auffret** was born in France in 1966. He graduated in automated systems and computer sciences from the University of Western Brittany (Universit de Bretagne Occidentale, UBO), and received the PhD degree in electronics from the same university.

From 1988 to 1993 he worked at Orca instrumentation, Brest. In 1993, he joined the French Research Institute for Exploration of the Sea (IFREMER). In 2013, he joined the Underwater Acoustic & Instrumentation laboratory at the Engineering School ISEN/Brest (Institut Supérieur de l'Electronique et du Numérique) as an Associate Professor in digital electronics and embedded systems. His current research interests include: marine and submarine instrumentation, unmanned surface vehicles (USV), data acquisition systems and sea bottom observatories.